Virologica Sinica 37 (2022) 938–941

Contents lists available at ScienceDirect

Virologica Sinica

journal homepage: www.keaipublishing.com/en/journals/virologica-sinica
www.virosin.org

Letter

Structures of SARS-CoV-2 spike protein alert noteworthy sites for the potential approaching variants

Xiaorui Xing [a,b,c,1], Lei Wang [c,d,1], Zhen Cui [c,d,1], Wangjun Fu [c,d,1], Tao Zheng [c,d], Lili Qin [e], Pingju Ge [e], Aidong Qian [a,b,*], Nan Wang [c,*], Shuai Yuan [f,*]

[a] College of Veterinary Medicine, Jilin Agricultural University, Changchun, 130118, China
[b] College of Animal Science and Technology, Jilin Provincial Engineering Research Center of Animal Probiotics, Key Lab of Animal Production, Product Quality and Security, Joint Laboratory of Modern Agricultural Technology International Cooperation, Ministry of Education, Jilin Agricultural University, Changchun, 130118, China
[c] CAS Key Laboratory of Infection and Immunity, National Laboratory of Macromolecules, Institute of Biophysics, Chinese Academy of Sciences, Beijing, 100101, China
[d] University of Chinese Academy of Sciences, Beijing, 100101, China
[e] Acrobiosystems, Beijing, 100101, China
[f] State Key Laboratory of Virology, Wuhan Institute of Virology, Chinese Academy of Sciences, Wuhan, 430071, China

Dear Editor,

The COVID-19 pandemic, which is caused by severe acute respiratory syndrome coronavirus 2 (SARS-CoV-2), has led to millions of lives lost worldwide. The trimeric spike protein (S) decorating the membrane surface of the infectious virion is responsible for the attachment and entry by binding to the receptor angiotensin-converting enzyme 2 (ACE2) in the early replication cycle (Zhou P. et al., 2020). Two subunits S1 and S2 are included in the trimeric glycoprotein. S1 subunit is composed of the N-terminal domain (NTD), receptor-binding domain (RBD), and C-terminal domains (CTD0, CTD1, and CTD2) and interacts with ACE2 through RBD. S2 subunit plays key roles in the viral-cell membrane fusion and is divided into fusion peptide (FP), fusion-peptide proximal region (FPPR), heptad repeat 1 (HR1), central helix (CH), connector domain (CD), heptad repeat 2 (HR2), trans-membrane segment (TM) and the cytoplasmic tail (CT) (Hoffmann et al., 2020; Zhang et al., 2021). After the RBD binding to the receptor, the fusion peptide (FP) of the S2 subunit inserts into the cell membrane. Subsequently, the HR1 domain is exposed and forms a helix-bundle together with the HR2 domain. Finally, the viral envelope and cell membrane draw close to each other, leading fusion and entry to happen (Cai et al., 2020; Walls et al., 2017). The mutations or deletions in RBD and NTD of different variants facilitate the immune evasion progress and affect the viral infectivity (Harvey et al., 2021). Whereas some mutations in other domains can also change the infectivity, such as D614G that is in the CTD2 domain. D614G mutation is proved to increase viral infectivity and became dominant quickly worldwide (Korber et al., 2020; Zhang et al., 2020). Here in our study, we found that mutation T859N involved in supporting the upper domains can increase the interaction between the protomers, induce the local conformational changes and induce the upper domains to shift. It further reminds us to pay attention to the mutations in the potential approaching variants which are outside of RBD and NTD and still can alter the conformation, especially the mutations in FPPR and 630 loop motif.

We determined the cryo-EM structures of the spike complex in both open and closed states from different variants including Lambda, Mu, C.1.2, and B.1.620 (Fig. 1A, Supplementary Figs. S1–3). In the closed state, the RBD is half embedded on the top of the glycoprotein complex in a threefold-symmetry manner. While in the open state, one RBD projects out and gets prepared for the interaction with ACE2. Only one "standing-up" RBD is observed in each variant in our reconstruction (Fig. 1A).

Like other variants, most of the mutations in the S protein of Lambda, Mu, C.1.2, and B.1.620 variants are within the RBD and NTD (Fig. 1B). These mutations can facilitate the virion to escape from antibody recognition. All the four variants share the D614G mutation which is dominant worldwide now. Intriguingly, Lambda and C.1.2 variants both have the same T859N mutation which is neighboring D614G. In Mu and B.1.620 variants, no mutation or deletion is found near residue G614 (Fig. 1B). Moreover, a mutation H655Y, which is shared among C.1.2, Gamma, and Omicron, interacts with the neighboring glycan. Considering the important roles of the glycans on the S complex, the H655Y mutation may also contribute to changing the viral infectivity (Fig. 1B and Supplementary Fig. S4).

Although there is a crowd of mutations found among these variants, the overall structures of the closed state S complex from different variants resemble each other in both S1 and S2 subunits. The most rigid part, mainly comprised of a long helix-bundle in the S2 subunit, is almost identical among the variants (Fig. 1C and D). The closed state S complex of the Delta variant that we previously reported also keeps consistent

* Corresponding authors.
E-mail addresses: qianaidong0115@163.com (A. Qian), wangnan161@ibp.ac.cn (N. Wang), yuanshuai@wh.iov.cn (S. Yuan).
[1] Xiaorui Xing, Lei Wang, Zhen Cui and Wangjun Fu contributed equally to this work.

https://doi.org/10.1016/j.virs.2022.11.003
Received 30 June 2022; Accepted 4 November 2022
Available online 8 November 2022

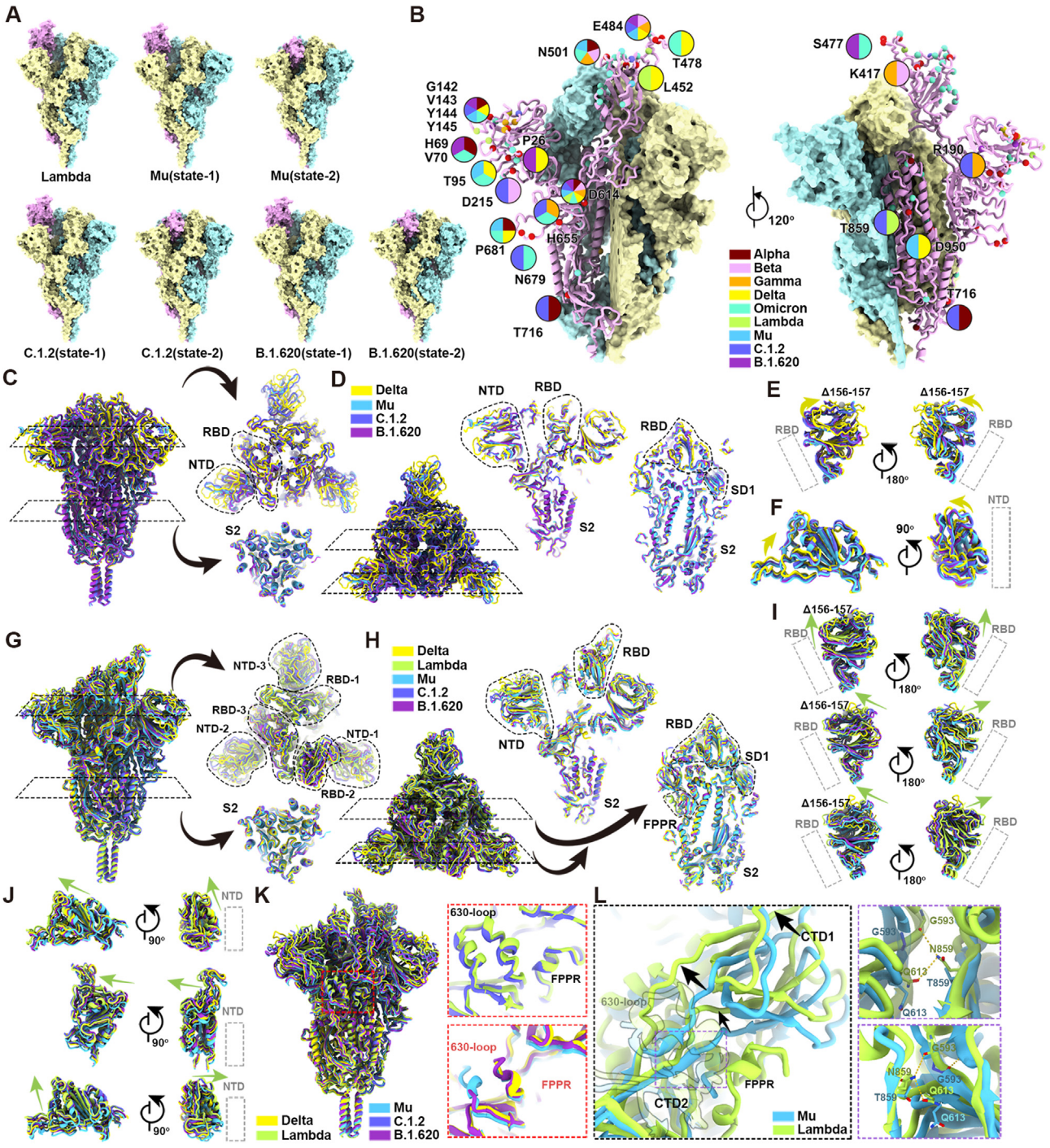

Fig. 1. Structural basis for SARS-CoV-2 spike conformational changes among variants. Overall structures of SARS-CoV-2 spike proteins from different variants with states labeled and three protomers are colored in pink, yellow, and cyan. **B** A scheme presentation of mutations of SARS-CoV-2 variants. The protomer with RBD in the open state is shown in cartoon. The residues are highlighted with spheres and colored, respectively. The positions of residue with two or more mutations are marked with red balls and labeled with pies to represent all the variants with these mutations. **C**–**D** Superimpositions of SARS-CoV-2 Delta (PDB: 7WG8), Mu, C.1.2, and B.1.620 variants spike protein with all RBD in close state. The dash line boxes show the locations of sectional views and the regions with distinct movements are highlighted with black dash lines. **E**–**F** Superimpositions of RBD and NTD from the variants in (**C**) and (**D**). The corresponding location of RBD and NTD are labeled with grey dash line boxes, respectively. The movements of RBD and NTD are labeled with yellow arrows. **G**–**H** Superimpositions of SARS-CoV-2 Delta, Lambda, Mu, C.1.2, and B.1.620 variants spike protein with one RBD in the open state. The RBDs and NTDs are named and labeled. The dash lines stay consistent with (**C**–**D**). **I**–**J** Superimpositions of NTD-1 (top), NTD-2 (middle), and NTD-3 (bottom) in (**I**) and RBD-1 (top), RBD-2 (middle), and RBD-3 (bottom) in (**J**). The relative locations of RBDs/NTDs are labeled with grey dash line boxes and the movements of NTD/RBD of Lambda and C.1.2 relative to the others are labeled with green arrows. **K** Superimpositions of SARS-CoV-2 Delta, Lambda, Mu, C.1.2, and B.1.620 with NTD-3 and NTD-2 in front view. FPPR and 630-loop of variants are highlighted with the zoom-in view. **L** Superimposition of CTD1/2s of Mu and Lambda variant. The location of the 630-loop is shown in silhouette. Movements of the loops are labeled with black arrows. The interactions are highlighted with the zoom-in view.

(Fig. 1C and D) (Cui et al., 2022). Although the NTD of Mu, C.1.2, and B.1.620 variants fit well with each other, we observed a clear shift in the Delta variant NTD (Fig. 1E). The smaller loop in Delta variant NTD that is shortened by the two residues (156–157 aa) deletion leads to the distortion of the following beta-strand. As a result, the neighboring beta-sheet is warped gradually and finally leads the whole NTD to shift obviously (Fig. 1E). The half-embedded RBD domains also share a similar organization. The main secondary structures in RBD keep in similar positions. There is also some local shifting which is probably induced by the local mutations (Fig. 1F).

Similar to the closed states, the S2 subunits from different variants align well with each other in the open states (Fig. 1G and H). However, conformational differences can be observed in the S1 subunits. These five variants can be divided into two groups based on their differences. The RBD and NTD from Lambda are similar to those of C.1.2, while Mu, Delta, and B.1.620 resemble to each other in these two domains (Fig. 1G and H). The RBD and NTD of Lambda and C.1.2 are lifted higher than those of Mu, Delta, and B.1.620 (Fig. 1I and J). From the top view, there is an anti-clockwise rotation of the Lambda and C.1.2 RBD and NTD relative to that of Mu, Delta, and B.1.620 (Fig. 1H). These conformational rotations and shifts in the overall upper region of the S complex between these two classes are probably less affected by the mutations in RBD and NTD especially considering the variety of the mutations and deletions in these two domains. Instead, some mutation(s) involved in linking the S1 and S2 subunits may be responsible for the distinct conformational differences. Also, these structural variances indicate that the trimeric spike complex is more stable in the closed state, and more flexible in the open state (Fig. 1C–J).

The FPPR that plays an important role in the membrane fusion progress locates in the section connecting the S1 and S2 subunits. We noted that there is a substitution for threonine (T) by asparagine (N) at position 859 in FPPR in S protein of Lambda and C.1.2, whereas it still holds a threonine (T) at position 859 in S protein of Mu, Delta and B.1.620 variants (Fig. 1B). Intriguingly, the substitution T859N happens not far from the well-known substitution D614G sterically. The D614G change breaks a salt bridge between D614 and K854 which belongs to FPPR and is proven to increase the viral infectivity (Cai et al., 2020; Korber et al., 2020; Zhou T. et al., 2020). Intriguingly, in the open state S protein of Lambda and C.1.2 variants, the N859 builds new interactions between the FPPR and the neighboring 630 loop motif (aa 620–640) of CTD2 (Fig. 1K). N859 of the protomer with RBD standing interacts with G593 and Q613 from CTD2 of adjacent protomer whose RBD lays down, which recovers the interaction attenuated by D614G mutation (Fig. 1L). Because of the enhanced interaction between CTD2 and FPPR, the 630 loop motif can be well reconstructed in Lambda and C.1.2. On the contrary, the 630 loop motif is still partly invisible in Delta, Mu, and B.1.620 since T859 cannot reach the residues of CTD2 in these variants (Fig. 1K and L). The packing of the 630 loop motif further induces local conformational changes. There is a short beta-sheet comprised of residents 317–319 from the CTD0 domain (a small domain connecting NTD and RBD) and residents 592–594 from the CTD2 domain in Delta, Mu, and B.1.620 variants. In the lambda and C.1.2 variants, the well-packed 630 loop motif impairs the formation of the short beta-sheet. Instead, there are two separated loops observed. The new loop in the CTD0 domain (aa 317–323) is further lifted upside (Fig. 1L). As a result, the following beta-sheet in RBD is also elevated (Fig. 1K). These conformational changes would probably explain why the whole upper region of Lambda and C.1.2 is lifted and rotated. These differences also suggest that the kinetic barriers will probably make the transition of RBD between standing and sitting more difficult in Lambda and C.1.2 variants. These conformational differences do not decrease the viral infection directly by lowering the ratio of open state RBD, since it is also more difficult for the standing RBD to transit to sitting state. This is proved by the *in vitro* binding affinity assays. The majority of the residues of S protein that interact with ACE2 in Lambda and Mu are conserved and the binding affinity of trimeric S complex of Lambda is slightly lower than that of Mu strain (Supplementary Fig. S5). No obvious difference is observed. These results are consistent with the pseudovirus assays reported previously, in which the infectivity of the T859N mutation was similar to (just slightly lower than) that of the parental pseudovirus (Kimura et al., 2022).

In summary, this work reveals the conformational flexibility of the SARS-CoV-2 S complex by analyzing a series of cryo-EM structures of the S complex in both open and closed states from multiple variants. Moreover, the conformational differences induced by the substitution T859N in FPPR suggest that mutations outside of RBD and NTD can affect the overall structure of the trimeric S complex. Our results here remind us to pay more attention to mutations outside the RBD and NTD, especially the substitutions or deletions in the FPPR and 630 loop motif, in the potential upcoming variants in the future.

Footnotes

The cryo-EM data were collected at the Center for Biological imaging (CBI) in the Institute of Biophysics (IBP) of the Chinese Academy of Sciences (CAS). We thank Acrobiosystems for critical reagents and technical support. This work was supported by funding from Beijing Natural Science Foundation-Haidian Primitive Innovation Joint fund (L192008), the National Key R&D Program (2020YFA0707500, 2018YFA0900801, 2021YFA1301400) and the National Natural Science Foundation of China (31872730 and 32070947). The authors declare that they have no competing interests. This article does not contain any studies with human or animal subjects performed by any of the authors.

Coordinates and structure factors have been deposited in the Protein Data Bank. The atomic coordinates of spike proteins of C.1.2, B.1.620, Mu, and Lambda variants have been submitted to Protein Data Bank with accession codes 7YBN (C.1.2 open state), 7YBM (C.1.2 close state), 7YBL (B.1.620 close state), 7YBK (B.1.620 open state), 7YBJ (Mu close state), 7YBI (Mu open state), 7YBH (lambda), respectively. Cryo-EM maps in this letter have been deposited at Electron Microscopy Data Bank with accession codes EMD-33727 (C.1.2 open state), EMD-33726 (C.1.2 close state), EMD-33725 (B.1.620 close state), EMD-33724 (B.1.620 open state), EMD-33723 (Mu close state), EMD-33722 (Mu open state), EMD-33721 (lambda), respectively. Supplementary data to this article can be found online at https://doi.org/10.1016/j.virs.2022.11.003.

References

Cai, Y., Zhang, J., Xiao, T., Peng, H., Sterling, S.M., Walsh Jr., R.M., Rawson, S., Rits-Volloch, S., Chen, B., 2020. Distinct conformational states of SARS-CoV-2 spike protein. Science 369, 1586–1592.

Cui, Z., Liu, P., Wang, N., Wang, L., Fan, K., Zhu, Q., Wang, K., Chen, R., Feng, R., Jia, Z., Yang, M., Xu, G., Zhu, B., Fu, W., Chu, T., Feng, L., Wang, Y., Pei, X., Yang, P., Xie, X.S., Cao, L., Cao, Y., Wang, X., 2022. Structural and functional characterizations of infectivity and immune evasion of SARS-CoV-2 Omicron. Cell 185, 860–871.e13.

Harvey, W.T., Carabelli, A.M., Jackson, B., Gupta, R.K., Thomson, E.C., Harrison, E.M., Ludden, C., Reeve, R., Rambaut, A., Consortium, C.-G.U., Peacock, S.J., Robertson, D.L., 2021. SARS-CoV-2 variants, spike mutations and immune escape. Nat. Rev. Microbiol. 19, 409–424.

Hoffmann, M., Kleine-Weber, H., Pöhlmann, S., 2020. A multibasic cleavage site in the spike protein of SARS-CoV-2 is essential for infection of human lung cells. Mol. Cell 78, 779–784.e775.

Kimura, I., Kosugi, Y., Wu, J., Zahradnik, J., Yamasoba, D., Butlertanaka, E.P., Tanaka, Y.L., Uriu, K., Liu, Y., Morizako, N., Shirakawa, K., Kazuma, Y., Nomura, R., Horisawa, Y., Tokunaga, K., Ueno, T., Takaori-Kondo, A., Schreiber, G., Arase, H., Genotype to Phenotype Japan, C., Motozono, C., Saito, A., Nakagawa, S., Sato, K., 2022. The SARS-CoV-2 Lambda variant exhibits enhanced infectivity and immune resistance. Cell Rep. 38, 110218.

Korber, B., Fischer, W.M., Gnanakaran, S., Yoon, H., Theiler, J., Abfalterer, W., Hengartner, N., Giorgi, E.E., Bhattacharya, T., Foley, B., Hastie, K.M., Parker, M.D., Partridge, D.G., Evans, C.M., Freeman, T.M., de Silva, T.I., McDanal, C., Perez, L.G., Tang, H., Moon-Walker, A., Whelan, S.P., LaBranche, C.C., Saphire, E.O., Montefiori, D.C., 2020. Tracking changes in SARS-CoV-2 spike: evidence that D614G increases infectivity of the COVID-19 virus. Cell 182, 812–827.e819.

Walls, A.C., Tortorici, M.A., Snijder, J., Xiong, X., Bosch, B.J., Rey, F.A., Veesler, D., 2017. Tectonic conformational changes of a coronavirus spike glycoprotein promote membrane fusion. Proc. Natl. Acad. Sci. U. S. A. 114, 11157–11162.

Zhang, J., Xiao, T., Cai, Y., Chen, B., 2021. Structure of SARS-CoV-2 spike protein. Curr. Opin. Virol. 50, 173–182.

Zhang, L., Jackson, C.B., Mou, H., Ojha, A., Peng, H., Quinlan, B.D., Rangarajan, E.S., Pan, A., Vanderheiden, A., Suthar, M.S., Li, W., Izard, T., Rader, C., Farzan, M.,

Choe, H., 2020. SARS-CoV-2 spike-protein D614G mutation increases virion spike density and infectivity. Nat. Commun. 11, 6013.

Zhou, P., Yang, X.L., Wang, X.G., Hu, B., Zhang, L., Zhang, W., Si, H.R., Zhu, Y., Li, B., Huang, C.L., Chen, H.D., Chen, J., Luo, Y., Guo, H., Jiang, R.D., Liu, M.Q., Chen, Y., Shen, X.R., Wang, X., Zheng, X.S., Zhao, K., Chen, Q.J., Deng, F., Liu, L.L., Yan, B., Zhan, F.X., Wang, Y.Y., Xiao, G.F., Shi, Z.L., 2020. A pneumonia outbreak associated with a new coronavirus of probable bat origin. Nature 579, 270–273.

Zhou, T., Tsybovsky, Y., Gorman, J., Rapp, M., Cerutti, G., Chuang, G.Y., Katsamba, P.S., Sampson, J.M., Schön, A., Bimela, J., Boyington, J.C., Nazzari, A., Olia, A.S., Shi, W., Sastry, M., Stephens, T., Stuckey, J., Teng, I.T., Wang, P., Wang, S., Zhang, B., Friesner, R.A., Ho, D.D., Mascola, J.R., Shapiro, L., Kwong, P.D., 2020. Cryo-EM structures of SARS-CoV-2 spike without and with ACE2 reveal a pH-dependent switch to mediate endosomal positioning of receptor-binding domains. Cell Host Microbe 28, 867–879.e865.